

The neural control of movement must contend with trajectory-specific and nonlinearly distorted manifolds of afferent muscle spindle activity

Jasmine A. Berry*, Robert Ritter III†, Akira Nagamori‡, Francisco J. Valero-Cuevas†‡

*Department of Computer Science

†Department of Biomedical Engineering

‡Division of Biokinesiology and Physical Therapy

Brain-Body Dynamics Lab, University of Southern California

Los Angeles, California

Email: valero@usc.edu

Abstract—We introduce the concept of trajectory-specific sensory manifolds. They are the unique multidimensional and time-varying combinations of afferent signals that obligatorily emerge during a limb movement. We use the example of muscle spindles (i.e., the muscle’s proprioceptors for length and velocity) that arise during movements of an arm (a planar 2-DOF 6-muscle model) during the production of straight, curved and oscillatory hand movements. Through the use of parallel coordinates, we visualize the high-dimensional evolution of the afferent signaling across muscles and tasks. We demonstrate that a given movement gives rise to a distinct sensory manifold embedded in the 12-D space of spindle information that is largely independent of the choice of muscle coordination strategy. Given that muscle lengths and velocities are fully determined by joint kinematics, such manifolds provide a rich set of information to use in its control.

Keywords—proprioception; biomechanics; sensorimotor; neural; muscle spindle; kinematics; afferent signals; self-awareness

I. INTRODUCTION: HOW THE BODY BUILDS THE BRAIN

Sensorimotor control research, both past and ongoing, has made efforts to predominately provide evidence for how the brain shapes the body [1], [2]. However, the counterpart to these works, how the body shapes the brain [3], [4], [5] is not as extensively considered. Often not taken into account are sensory states and their effects on building the brain’s body awareness which is necessary for involuntary and voluntary behavior. Here we investigate the flow of information underlying limb movements, and explore its significance to perceptual learning. We begin our work in this area by defining the concept of a feasible sensory set for a given movement.

Our study follows the work of [6], [7], [8] that developed a theoretical framework for all possible body accelerations, activations and torques for a given tasks (e.g., feasible acceleration, activation, torque or force sets). By extension, we can also speak of a feasible sensory set (FSS). In the case of muscle spindle afferents—which sense muscle lengths and velocities—the FSS defines the set of sensory signals that can emerge for a given limb posture or movement. In particular, given that muscle lengths and velocities are geometrically

defined by joint angles and angular velocities [9] then a given posture or limb movement will also prescribe the spindle afferent signals. Given a motor task, and a definition of available sensory information, we sought to define the associated manifold of spindle afferent signals that define its FSS.

II. METHODS AND ANALYSES

We used a simplified tendon-driven arm model where simulated muscles pull on tendons that cross, and therefore actuate, kinematic Degrees of Freedom (DOFs). The planar model had six muscles, two links (upper arm and forearm) and two DOFs (Shoulder Flexion/Extension (SFE) and elbow flexion/extension (EFE)).

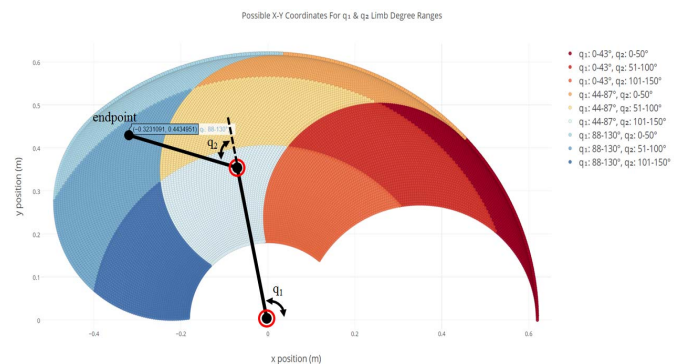


Fig. 1. For the Static Case, all possible x-y coordinates for q_1 and q_2 degree ranges. q_1 and q_2 were constrained within ranges of motion 0-130° and 0-150°, respectively. Location of the SFE joint remains fixed at the origin (0, 0).

The lengths of the upper arm and forearm were 0.35 and 0.27 meters, respectively, with musculature comparable to that of [10]. A combination of paired antagonistic muscles formed the tendon routing of a right arm appendage: deltoid anterior (monoarticular shoulder flexor), deltoid posterior (monoarticular shoulder extensor), biceps brachii (biarticular elbow flexor), triceps brachii (biarticular elbow extensor), brachialis (monoarticular elbow flexor), and anconeus

(monoarticular elbow extensor). The study was partitioned in two parts beginning with kinematic calculations of an arm during a task to derive limb joint angles and endpoint locations, and then applying those metrics to the spindle model for observation of afferent signaling. Incorporating modeled muscle parameters of optimal fiber lengths L_o , change in angle δq , and constant moment arm values r from upper extremity analyses [11] allowed the initial computation of tendon excursion (change in length of musculotendon) values, as shown in (1).

$$\delta s = r \delta q \quad (1)$$

We investigated how limb movements affect two chief elements of muscle afferentation for muscle length/contractile velocity (Table 1). Using inverse kinematics [12], a Static Case was used to find all possible discrete positions our modeled arm can achieve (Fig. 1). Variations in proprioceptive signaling are shown to be dependent on task constraints as studies have revealed active movements tending to report more accurate proprioceptive approximations [13], [14], which led us to incorporate a case with continuous arm movement in dynamic settings. The Dynamic Case consists of specific trajectories the

TABLE I. AFFERENT MUSCULOSKELETAL MECHANORECEPTORS

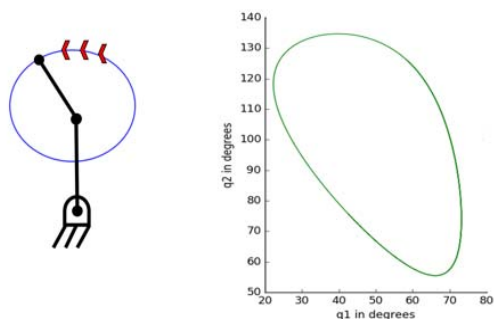
Receptor Type	Axon Fiber	Fiber Name	Transducer Modality
Muscle spindle primary ^a	A α	Ia	Muscle length and speed
Muscle Spindle secondary ^b	A β	II	Muscle stretch

^a. Classification of afferents and their respective function for detecting deformation of muscle tissue and transducing those signals into electrical responses. Fastest conduction speed and fiber diameter, A α (72-120 m/s) has the thickest myelination,

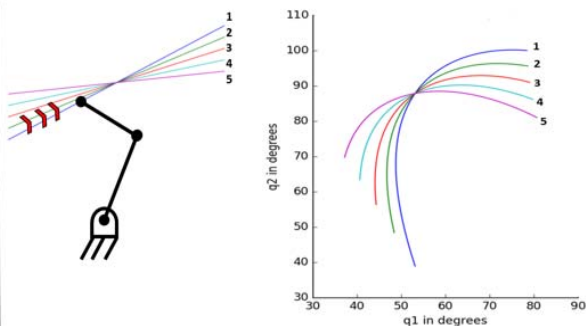
^b. A β (36-72 m/s) possess thinner myelinated axons [15]

arm follows over a set time frame that can be modified via the Speed Factor parameter. As the Speed Factor increases so does the velocity of the movement under observation. Within the Dynamic Case, we evaluated our arm limb moving in several tasks starting with the Circle trajectory (in counterclockwise direction) as illustrated in Fig. 2A. The Straight Linear trajectory task consisted of five distinct pathways on a plane for the arm to follow, each perturbed at the slope by a 0.1 decrement (Fig. 2B). The Oscillatory trajectory represented sinusoidal movement with an angular frequency of 6π , amplitude of .05m, and .35m vertical shift (Fig. 2C). And lastly, we defined the symmetrical lobe Lemniscate

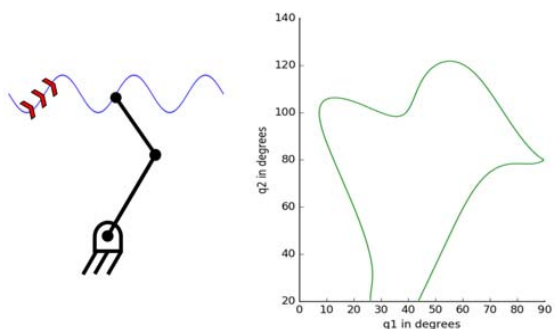
A. Circular Path Trajectory: Cartesian & Configuration Space



B. Straight Line Path Trajectory: Cartesian & Configuration Space



C. Oscillatory Path Trajectory: Cartesian & Configuration Space



D. Lemniscate Path Trajectory: Cartesian & Configuration Space

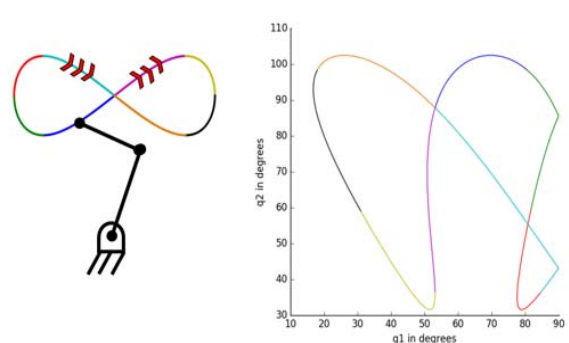


Fig. 2. Cartesian space and Configuration space of arm movement in directions indicated by the red cursors for A) the arm limb in action during the Circle Trajectory task in the counterclockwise direction. Configuration space illustrates the joint angles for 360 distinct postures. B) Arm limb in action during the Straight Linear Trajectory task in a left to right direction. Line 1 trajectory, in blue, sustains a slope of .5. Line 2 trajectory, in green, sustains a slope of .4. Lines 3-5 follow according with a negative .1 gradient. Configuration Space illustrates the joint angles for 1,000 distinct postures. C) Arm limb in action during the Oscillatory Trajectory task in a left to right direction. Configuration Space illustrates the joint angles for 1,000 distinct postures from the leftmost to rightmost point along the trajectory. D) Arm limb in action for Lemniscate Trajectory task with symmetrical lobes. The depicted path is partitioned according to color scheme for mapping the end-effector location in Cartesian coordinates to the joint angles illustrated in the Configuration Space, which illustrates for 1,000 distinct postures.

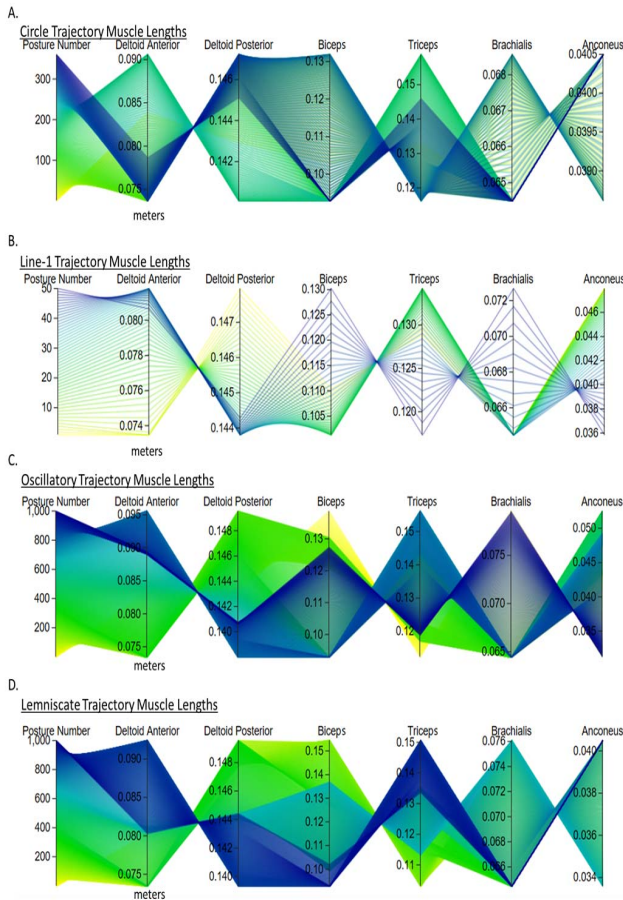


Fig. 3. Six-dimensional representation of change in muscle length along four trajectories of the Dynamic Case. Color gradient depicts initial postures (yellow), intermediate postures (green), and concluding postures (blue). A) Muscle length values (meters) during Circle Trajectory task. 360 postures were examined ranging from Posture 1 at 0 radians to Posture 360 at 2π radians. Direction of movement along the trajectory is counter-clockwise. B) Muscle length values during Line 1 Trajectory task. 50 postures were examined ranging from Posture 1 at the leftmost point on the line to Posture 50 at the rightmost point. Lines 2-5 follow the same paradigm of movement sequences just with an altered slope. C) Muscle length values during Oscillatory Trajectory task. 1,000 postures were examined ranging from Posture 1 at the leftmost point on the sinusoidal wave to Posture 1,000 at the rightmost point. D) Muscle length values during Lemniscate Trajectory task for 1000 postures.

(i.e., “figure of eight”) trajectory [16] (Fig. 2D) using the mathematical expressions shown in (2) and (3). It must be noted that the derived configuration spaces only disclose exclusive Θ values for q_1 and q_2 despite the possibility of a multiplicity of joint angles producing the same end-effector position.

$$x = \alpha \cos(t) / (1 + \sin^2(t)) \quad (2)$$

$$y = \alpha \sin(t) \cos(t) / (1 + \sin^2(t)) \quad (3)$$

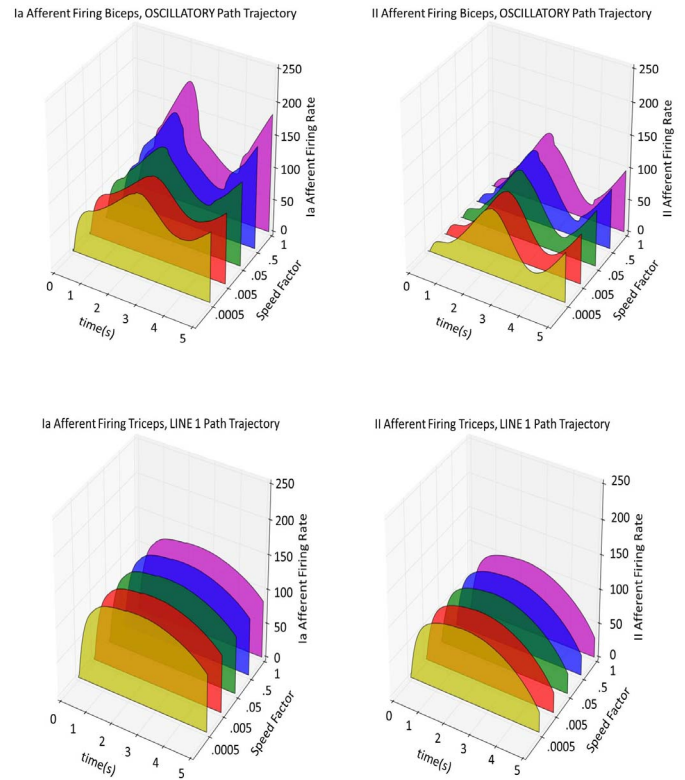


Fig. 4. Velocity speeds versus afferent signals in Group Ia (left) and II (right). Five values were used for the Speed Factor, with value 1 signaling the fastest speed across the task. Top row: Afferent firing in the biceps muscle for the Oscillatory task shows slight oscillations with increasing speed. Bottom row: Afferent Firing for the triceps muscle shows a uniform and smooth signal throughout the span of Speed Factors.

After solving for the joint and limb kinematics, we utilized a computational sub-model to simulate the biological spindle as observed in mammalian muscles, namely that of the cat [17], [18] which has also been used in human simulations [19], [20]. Action potentials in pulses per second (pps) were generated for primary (Ia) and secondary (II) afferents based on the interactions of the intrafusal fibers (chain, bag₁, bag₂). The first analysis that we performed examined whether afferent signals are dependent on muscle velocity throughout a task. We varied the Speed Factor in the system by a combination of values ranging in ascending speed: 0.0005, 0.005, 0.05, 0.5, and 1. One-way analysis of variance (ANOVA) of the measured spindle signals under these varying velocities tested whether there was a significant difference between the group output values. Velocities were categorical and set as the independent variable while the spindle firings served as the continuous dependent variable. Our second analysis developed the high-dimensional sensory space for Ia and II afferent signaling to extract the sensory afferent sets for the Dynamic tasks.

TABLE II. VELOCITY SIGNIFICANCE IN AFFERENTS (ANOVA P-VALUES)

	Fiber Type	Circle	Line 1-5 (\bar{x})	Oscillatory	Lemniscate
Deltoid A.	Ia	0.049	0.249	<0.001	<0.001
	II	0.830	0.861	<0.001	<0.001
Deltoid P.	Ia	0.538	0.999	<0.001	<0.001
	II	0.999	0.999	0.087	<0.001
Biceps	Ia	<0.001	0.981	<0.001	<0.001
	II	0.213	0.999	<0.05	<0.001
Triceps	Ia	<0.001	0.753	<0.001	<0.001
	II	<0.01	0.950	<0.001	<0.001
Brachialis	Ia	0.362	0.999	<0.001	<0.001
	II	0.850	0.999	0.072	<0.001
Anconeus	Ia	<0.001	0.474	<0.001	<0.001
	II	<0.001	0.967	<0.001	<0.001

III. RESULTS

A. Kinematics Assessment

Parallel coordinates were used to clearly illustrate the multi-dimensional change in muscle lengths for each posture during the tasks of the Dynamic Case. Such assessment was conducted to verify the efficacy of our model to ensure isometric, concentric and eccentric contractions according to physiological expectations [21], [22]. As shown in Fig. 3, we sampled n postures along each trajectory (i.e., task) and integrated δs from the initial posture. The three pairs of antagonistic muscles showed the expected concentric and eccentric contractions along their respective continuous trajectories. The muscle lengths were differentiated to derive the obtain their respective velocities and accelerations, which served as direct input parameters to each spindle model.

B. Afferent Signaling Dependent on Muscle Velocity

We expected that increased muscle velocities would affect spindles, and therefore, “body sense” in a heavily nonlinear way. Fig. 4 provides a sample of our observations. We detected the presence of perturbations in the Circle, Oscillatory, and Lemniscate; prospectively owing to the curvature of the trajectories which can induce abrupt changes in velocities. These finding corroborate observations from [17]. ANOVA tests revealed p-values for each muscle’s Ia and II afferent signals in each task of the Dynamic Case (Table 2). For those cases where $p \leq 0.05$, we rejected the null hypothesis that there was no difference between the defined sets of velocities and the resulting afferentation in each task. We detected significance in only particular groups of muscles in the Circle and Oscillatory trajectory tasks. The Straight Linear trajectory demonstrated no significant difference across all six muscles for each Speed Factor value (Fig. 4), while the Lemniscate

trajectory showed evidence for all muscles having affected afferentation.

C. Sensory Bounds According to Task Constraints

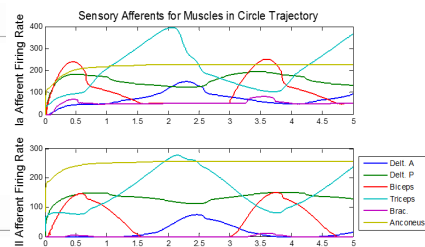
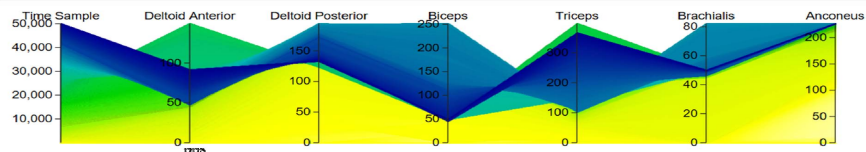
We also used parallel coordinates to describe Group Ia and II signals in the Dynamic Case with a reasonable duration of 5 seconds. Our sampling frequency (f_s) was set at 10 kHz (10,000 samples/second), resulting in 50,000 time samples throughout each trajectory. Fig. 5 presents the high-dimensional correlated relationships among afferent signals. To read these parallel coordinates, please note: 1) each axis is likely to have a different scale depending on the range of values reported for that muscle, 2) adjacent dimensions are more easily interpretable than non-adjacent dimensions, and 3) a web-based view provides the ability to interactively analyze subsets of activities of single muscles (as shown in Fig. 5 for the Line 1 & 5 trajectories). Therefore, we can explore the multivariate comparisons, patterns, and sequences that are unique to each muscle and trajectory. For example, for the Group II afferents of the Line 5 trajectory, we isolated the signals on the triceps muscle between 50-150pps. This revealed the associated firing rates for other muscles as related to the triceps: deltoid anterior 0-5 pps, deltoid posterior 80-130 pps, biceps 35-60+ pps, brachialis 0 pps, and anconeus 185-250+ pps. Similar introspections of signal bandwidth can be made for all other muscles. We also have the ability to trace and correlate any subset of physiological with kinematic variables such as velocities, accelerations, muscle lengths and stretch, and limb position in space.

To gain insight into the robustness of spindle afferents, we performed Monte Carlo simulation [23] for each of the six muscles with variation of the gamma static and dynamic fusimotor drive values. Within 100 trial iterations, boundary limits on both $\gamma_{dynamic}$ and γ_{static} were set to inclusively span 70 and 150 pps. Maximum standard deviation between any given set of the observed points approximated to 20pps, consequently resolving to a 10% deviation estimate of the signal as $\gamma_{dynamic}$ and γ_{static} were constrained at a constant rate of 100pps. This allows use to quantify how fusimotor activation, naturally, affects both motor capabilities and body sense. Furthermore, we present the importance of how each movement leads to a very specific set of sensory information. We can then propose the concept of feasible sensory manifolds, FSS, associated with each movement task.

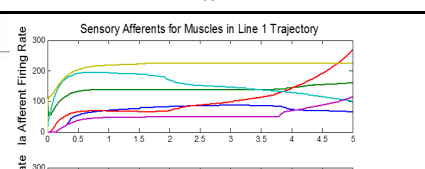
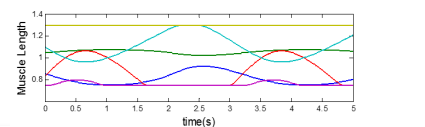
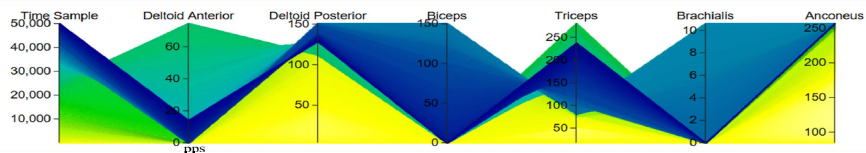
IV. DISCUSSION

How do our sensory signals shape the motor choices we make in daily life? In this paper, we addressed the body sense that arises from muscle spindle afferents, to enable future studies investigating how those same sensory signals affect the representation of our physical self and the actions we make. As per equation (1), we know that muscle excursions and velocities are completely determined by the time history of joint angles (so long as muscle tone prevents any muscle from being slack in any posture). Thus, every limb movement is associated with a unique set of specific sensory states, the FSS. As such we must consider how the nervous system obtains and processes sensory data to create a body sense that interacts

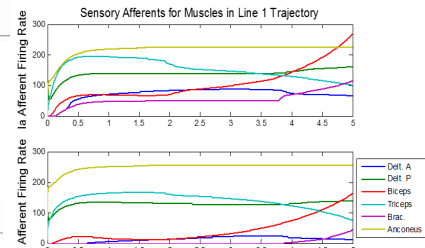
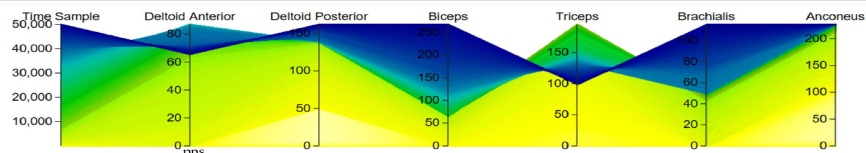
Ia Group Afferents for Circle Trajectory



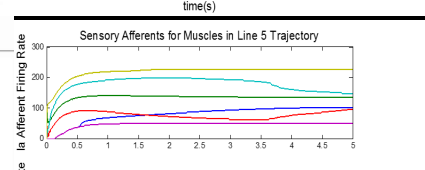
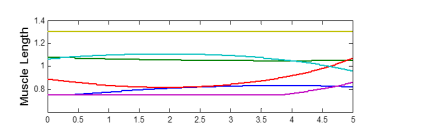
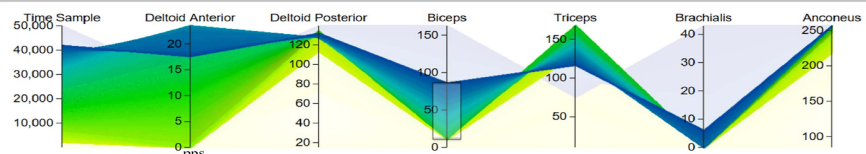
II Group Afferents for Circle Trajectory



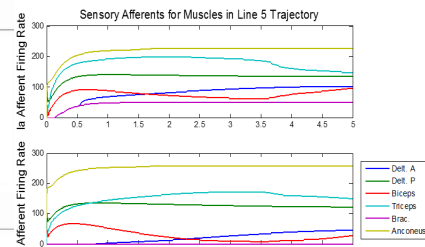
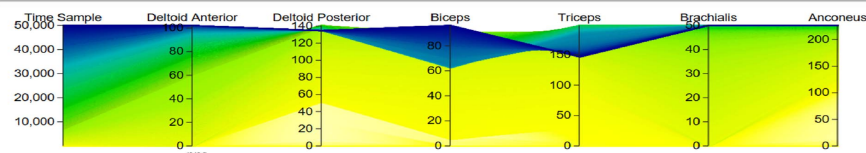
Ia Group Afferents for Line 1 Trajectory



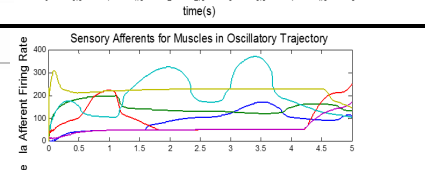
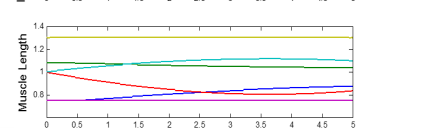
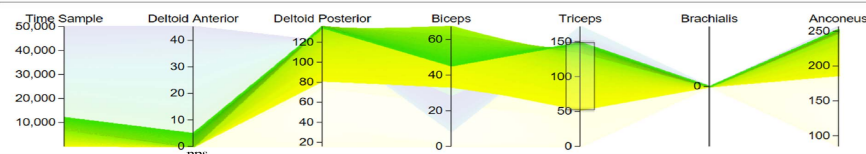
II Group Afferents for Line 1 Trajectory



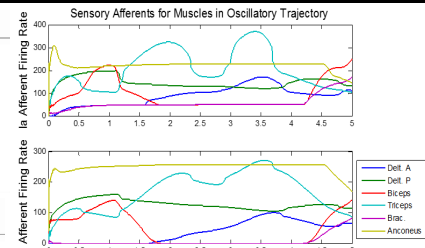
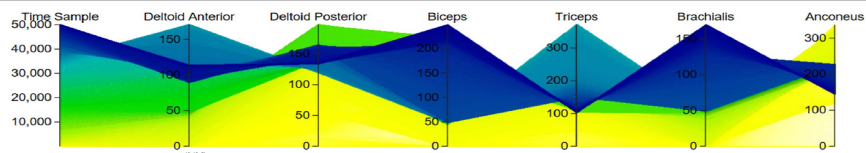
Ia Group Afferents for Line 5 Trajectory



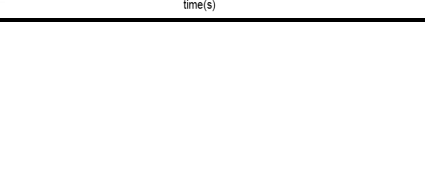
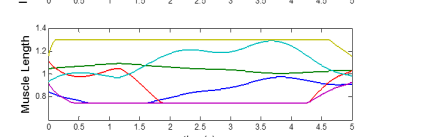
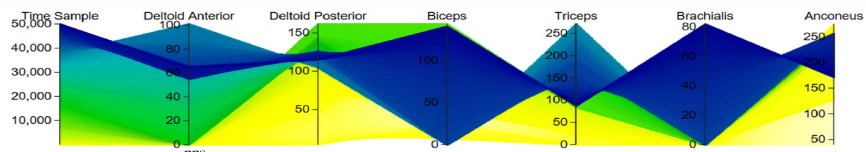
II Group Afferents for Line 5 Trajectory



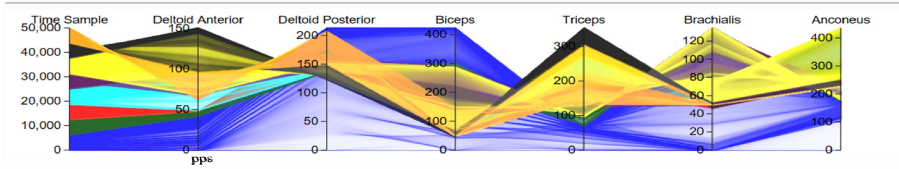
Ia Group Afferents for Oscillatory Trajectory



II Group Afferents for Oscillatory Trajectory



Ia Group Afferents for Lemniscate Trajectory



II Group Afferents for Lemniscate Trajectory

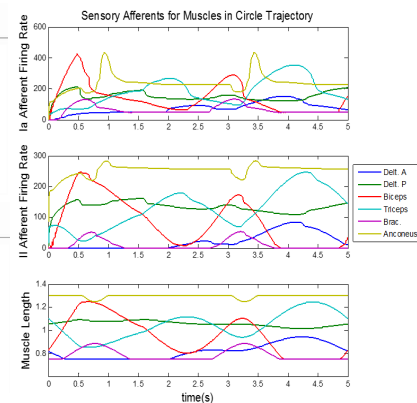
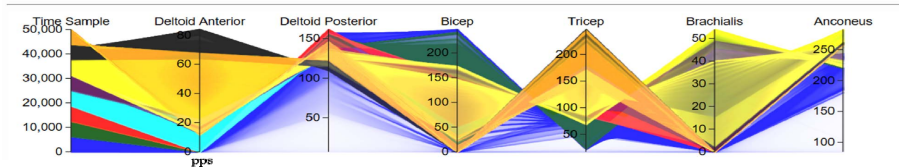


Fig. 5. Primary and secondary afferent space for the Circle, Line 1, Line 5, Oscillatory, and Lemniscate trajectory tasks marked by 50,000 samples in a time interval of 5 seconds from starting position to ending position along the prescribed trajectory. Left side: Parallel coordinates showing the activation of each group of muscle during a sampling range along the trajectory. Right side: Spindle afferentation of each muscle according to the range 0.75-1.3 of the optimal lengths. The parallel coordinate afferents for the Lemniscate trajectory is mapped with the color segments used in Fig. 2D. It can now be observed which location along the Lemniscate trajectory produces a certain afferentation value.

with explicit or implicit internal models of the body, and external influences on the body.

There are several perspectives on how sensory data (mostly visual) leads to perceptual states: the action-oriented theory of perception, which suggests that perception is the result of sensorimotor dynamics in an acting observer [24], [25], [26] and the dual-visual systems hypothesis, which advocates for independent streams of perception and action [27], [28], [29], [30], [31], [32]. Recognized predominantly as the Perception-Action Cycle [33], various methods developed from this framework may be utilized to replicate the decision making that occurs during the process of acquiring sensory modalities regarding the external world [34]. In the context of neuromechanics, we posit that sensory data obtained in any moment is dependent on the kinematic posture, position, and action task of the respective limb producing the sensory stimuli. Our present study delved into the consequences to sensory systems towards representation of high-dimensional observability to complement the controllability of muscle-driven limbs; specifically, within the mammalian muscle spindle. Our methods for obtaining these results can be employed towards systems such as robotics and brain-machine interfaces (BMIs) that are optimized on the limits of simulated neural drive obtained from sensory inputs.

The novelty in our work is that we are explicitly analyzing the unavoidable, physiologically basic, high-dimensional FSSs that accompany each movement. This is made possible by the use of interactive parallel coordinates. Velocity and acceleration were determined to be highly influential factors in perturbing sensory afferents for most arm muscles in the curvature-path Circle, Oscillatory, and Lemniscate task over the Straight Linear trajectory. This finding may provide explanation as to why in some cases motor control is more precise for straight trajectories (i.e. hand-drawing straight lines versus circular or curved shapes). Here we have shown and defined mapping space for sensory information regarding the muscle spindle. From our mappings in this research, it is possible to abstract a probability distribution of senses perceived or “felt” by the body at any given moment in a task.

As this work simulated a tendon-driven system, some discussion is warranted on the tendon’s function in a kinematic system. For our investigation, we have demonstrated a sensory set for an exclusive set of muscles with mechanically defined and unique excursions. However, as our joint angles were derived from inverse kinematics in conjunction with optimal muscle lengths, some speculation may be had on whether the addition of tendon elasticity would alter our findings. The sensory set and domain are prone to transformation as additional muscles are added to the system or if system parameters vary according to model specifications. For a tenable set of muscle excursions, our goal was to primarily reveal the evolution of afferentation for an idealized case where every muscle spindle’s afferents are dependent on the limb model and its characteristics. Due to the notion that a change in tendon length will also directly affect spindle-activity, we therefore concluded that our simulation was the best-case-scenario as tendon stretch would introduce additional nonlinearities. Moreover, adding Golgi tendon organs will extend the mechanically-driven dimensionality of the sensory signals, which necessarily complement other dominating senses such as haptics and vision. This work therefore sets a foundation to explore sensory domains from a variety of perspectives such as control, body sense, perception and physiologically-driven psychological identity.

ACKNOWLEDGMENTS

This research is supported by the Viterbi School of Engineering Fellowship and the National Institutes of Health under grant Awards Number R01 AR050520 and R01 AR052345. The authors would like to express gratitude to the members of the Brain-Body Dynamics Lab (BBDL) and course BME 504 Neuromuscular Systems at the University of Southern California for their suggestions on the direction of this research.

REFERENCES

- [1] T. Hanakawa, "Functional properties of brain areas associated with motor execution and imagery," *Journal of Neurophysiology*, vol. 89.2, pp. 989-1002, 2003.

- [2] R. Shadmehr, M. A. Smith, and J. W. Krakauer, "Error correction, sensory prediction, and adaptation in motor control," *Annual Review of Neuroscience*, vol. 33, pp. 89-108, 2010.
- [3] H. J. Chiel et al., "The Brain in Its Body: Motor Control and Sensing in a Biomechanical Context," *The Journal of neuroscience: the official journal of the Society for Neuroscience*, vol. 29.41 pp. 12807-12814, 2009.
- [4] N. Bernardi, M. Darainy, and D. J. Ostry, "Somatosensory contribution to the initial stages of human motor learning," *The Journal of Neuroscience*, vol. 35.42, pp. 14316-14326, 2015.
- [5] D. J. Ostry and P. L. Gribble. "Sensory plasticity in human motor learning," *Trends in Neurosciences*, vol. 39.2, pp. 114-123, 2016.
- [6] A. D. Kuo, and F. E. Zajac, "Human standing posture: multi-joint movement strategies based on biomechanical constraints," *Progress in Brain Research*, vol. 97, pp. 349-358, 1993.
- [7] F.J. Valero-Cuevas, "An integrative approach to the biomechanical function and neuromuscular control of the fingers," *Journal of Biomechanics*, vol. 38, pp. 673-684, 2005.
- [8] F. J. Valero-Cuevas, "A mathematical approach to the mechanical capabilities of limbs and fingers," *Progress in Motor Control*, Springer US, pp. 619-633, 2009.
- [9] F. J. Valero-Cuevas, B.A. Cohn, H. F. Yngvason, E. L. Lawrence, "Exploring the high-dimensional structure of muscle redundancy via subject-specific and generic musculoskeletal models," *J. Biomech*, 48(11), 2887-2896, 2015.
- [10] J. M. Inouye and F. J. Valero-Cuevas, "Muscle synergies heavily influence the neural control of arm endpoint stiffness and energy consumption." *PLoS Comput Biol* 12.2 e1004737, 2016
- [11] K. Holzbaur, W. Murray, S. L. Delp, "A model of the upper extremity for simulating musculoskeletal surgery and analyzing neuromuscular control," *Annals of Biomedical Engineering*, 33.6, 829-840, 2005.
- [12] L. Sciavicco, and B. Siciliano. *Modeling and control of robot manipulators*. Vol. 8. No. 0. New York: McGraw-Hill, 1996.
- [13] C. Fuentes and A. Bastian. "Where is your arm? Variations in proprioception across space and tasks," *Journal of neurophysiology*, vol. 103.1, pp. 164-171, 2010.
- [14] S. Zia, F. W. Cody, and D. J. O'Boyle, "Identification of unilateral elbow-joint position is impaired by Parkinson's disease," *Clin Anat*, vol. 15, pp. 23-31, 2002.
- [15] E. R. Kandel, J. Schwartz, and T. Jessell, *Principles of Neural Science* 4th ed. New York: McGraw-Hill, 2000.
- [16] M. Richardson and T. Flash. "Comparing smooth arm movements with the two-thirds power law and the related segmented-control hypothesis," *Journal of neuroscience* 22.18, pp. 8201-8211, 2002.
- [17] M. P. Mileusnic, I. E. Brown, N. Lan, and G. Loeb, "Mathematical models of proprioceptors. I. control and transduction in the muscle spindle," *Journal of Neurophysiology*, vol. 96(4), pp. 1772-1788, 2006.
- [18] M. P. Mileusnic, and G. E. Loeb. "Mathematical models of proprioceptors. II. Structure and function of the Golgi tendon organ." *Journal of Neurophysiology* 96.4, 1789-1802, 2006.
- [19] D. Song, et al., "Model-based sensorimotor integration for multi-joint control: development of a virtual arm model," *Annals of biomedical engineering*, vol. 36.6, pp. 1033-1048, 2008.
- [20] C. M. Laine, A. Nagamori, and F. J. Valero-Cuevas. "The Dynamics of Voluntary Force Production in Afferented Muscle Influence Involuntary Tremor." *Frontiers in Computational Neuroscience* 10, 2016.
- [21] M. A. LeMay, P. E. Crago, "Dynamic model for simulating movements of the elbow, forearm and wrist," *J. Biomechanics*, vol. 29, pp. 1319-1330, 1996.
- [22] H. E. J. Veeger, F. C. T. van der Helm, L. H. V. van der Woude, and G. M. Pronk, R. H. Rozendal, "Inertia and muscle contraction parameters for musculoskeletal modelling of the shoulder mechanism," *Journal of Biomechanics*, vol. 24, pp. 615-629, 1991.
- [23] S. Raychaudhuri, "Introduction to monte carlo simulation," *IEEE Winter Simulation Conference*, pp. 91-100, 2008.
- [24] J. J. Gibson, *The Senses Considered as Perceptual Systems*. Boston, MA: Houghton Mifflin, 1966.
- [25] Mandik, P. (2005). *Action-Oriented Representation*. In *Cognition and the Brain: The Philosophy and Neuroscience Movement*, (eds.) K. Akins and A. Brook (Cambridge: Cambridge University Press). 284-305.
- [26] Noë, A. (2004). *Action in perception*. Cambridge: MIT press.
- [27] M. A. Goodale and A. D. Milner, "Separate visual pathways for perception and action," *Trends in Neurosciences*, vol. 15(1), pp. 20-25, 1992.
- [28] M. A. Goodale and A. D. Milner, A.D. *Sight unseen: An exploration of conscious and unconscious vision*. Oxford: Oxford University Press, 2013.
- [29] P. Jacob and M. Jeannerod, *Ways of seeing: The scope and limits of visual cognition*. Oxford: Oxford University Press, 2003.
- [30] A. D. Milner and M. A. Goodale, *The visual brain in action*. Oxford: Oxford University Press, 2006
- [31] G. E. Schneider, "Two visual systems: brain mechanisms for localization and discrimination are dissociated by tectal and cortical lesions. *Science*," vol. 163, pp. 895-902, 1969.
- [32] C. Trevarthen, "Two mechanisms of vision in primates," *Psychological Research*, vol. 31(4), pp. 299-337, 1968.
- [33] U. Neisser. *Cognition and reality*. San Francisco, CA: W.H. Freeman and Company, 1976.
- [34] G. Loeb and J. Fishel. "Bayesian action&perception: Representing the world in the brain," *Frontiers in Neuroscience*, vol. 8, pp. 341, 2014.